PHOTONICS Research

On the upper limit of laser intensity attainable in nonideal vacuum

YITONG WU,[1,2,3] LIANGLIANG JI,[1,3,5] AND RUXIN LI[1,3,4,6]

[1]State Key Laboratory of High Field Laser Physics, Shanghai Institute of Optics and Fine Mechanics, Chinese Academy of Sciences, Shanghai 201800, China
[2]Center of Materials Science and Optoelectronics Engineering, University of Chinese Academy of Sciences, Beijing 100049, China
[3]CAS Center for Excellence in Ultra-intense Laser Science, Shanghai 201800, China
[4]ShanghaiTech University, Shanghai 201210, China
[5]e-mail: jill@siom.ac.cn
[6]e-mail: ruxinli@mail.siom.ac.cn

Received 2 December 2020; revised 4 February 2021; accepted 4 February 2021; posted 5 February 2021 (Doc. ID 416555); published 24 March 2021

The upper limit of the laser field strength in a perfect vacuum is usually considered as the Schwinger field, corresponding to $\sim 10^{29}$ W/cm^2. We investigate such limitations under realistic nonideal vacuum conditions and find that intensity suppression appears starting from 10^{25} W/cm^2, showing an upper threshold at 10^{26} W/cm^2 level if the residual electron density in chamber surpasses 10^9 cm^{-3}. This is because the presence of residual electrons triggers the avalanche of quantum electrodynamics cascade that creates copious electron and positron pairs. The leptons are further trapped within the driving laser field due to radiation reaction, which significantly depletes the laser energy. The relationship between the attainable intensity and the vacuity is given according to particle-in-cell simulations and theoretical analysis. These results answer a critical problem on the achievable light intensity based on present vacuum conditions and provide a guideline for future hundreds of petawatt class laser development.

https://doi.org/10.1364/PRJ.416555

1. INTRODUCTION

Ultrabright light sources have always been a major pursuit because of their applications in various research areas. At the moment, femtosecond lasers based on the chirped pulse amplification (CPA) technique [1] are regarded as the most reliable approach to realize the highest peak power. After being amplified, compressed, and focused, the peak laser intensity can reach up to 10^{22}–10^{23} W/cm^2 [2–5]. The 10 PW-class laser facilities, such as ELI [4] (ELI-NP [6] and ELI-BL [7]), Apollo [8], Vulcan [9], and SULF [10], aim at boosting the focused intensity by another tenfold. Ambitious plans of 100 PW-class have been proposed [11–13] worldwide, where the peak intensities of 10^{25} W/cm^2 are anticipated. Furthermore, efforts have also been paid in exploring new mechanisms to generate exawatt–zettawatt lasers [14–16]. At such extreme light intensities, particle acceleration towards 10–100 GeV for leptons [17] and 0.1–10 GeV/nucleon for ions [18–20] is to be expected. Nuclear physics [21–23] as well as lab astrophysics [24–26] will also benefit from these extreme laser sources. Laser–plasma interaction at such intensities enters a new regime where photon emission and radiation reaction become significant [27–34] and strong-field quantum electrodynamics (SF-QED) is necessary to account for the quantum effects [35–38]. It is further predicted that copious electron–positron pairs can be generated [37–55].

While high-power lasers are under fast development, a central question regarding the ultimate laser intensities researchers can build arises [56]. Basically, the upper limitation for laser intensity in an ideal vacuum condition is considered as the Schwinger field $E_s = 2\pi m_e^2 c^3/eh \sim 1.32 \times 10^{18}$ V/m [57]. The QED theory predicts that laser pulses of 10^{29} W/cm^2 can provide such field strength in several ways (tight focusing or coherent combining or others), such that they can transfer a large number of virtual particle pairs to real particles [58,59]. Meanwhile, the generated electron–positron pairs further lose their energies by radiating gamma photons. The laser energy is thus rapidly drained in vacuum [39]. Previous studies have shown that even a single pair produced in vacuum by a laser field can lead to rapid depletion of laser energy [44], i.e., the maximum light intensity is much smaller than 10^{29} W/cm^2 in vacuum. It points out that full depletion appears when the energy of generated pairs and photons is equivalent to the energy stored in the pulse, at $E \sim 6.6\alpha E_s \sim 0.05 E_s$ (corresponding to 5×10^{26} W/cm^2 for laser wavelength $\lambda = 800$ nm).

In reality, it is impossible to build a perfect vacuum environment for experiments. Typically, the vacuum electron

density in a chamber suitable for PW-class lasers is about 10^{11} cm^{-3}, provided by ordinary pumping technique (e.g., 10^{-3} Pa for SULF [10]). For laser power above 100 PW, the chamber volume is enlarged by more than tenfold, posing a great challenge to the pump. Another potential drawback is the existence of electrons extracted from optical components (focusing mirror, plasma mirror, etc.) by the passing laser fields. These residual electrons could serve as seeds to trigger the QED processes when the laser field surpasses a certain threshold. Specifically, during the laser–electron interaction, nonlinear Compton scattering [27] following $e + n\omega \rightarrow e + \gamma$ will occur, where electrons absorb multiple laser photons and emit high-energy γ photons. The radiated γ photons further interact with the strong laser field, generating electron–positron pairs via the nonlinear Breit–Wheeler process ($\gamma + n\omega \rightarrow e^+ + e^-$) [41]. These two reaction channels build up positive feedback, i.e., the amount of the pairs and γ photons will be avalanche-like amplified and deplete the laser significantly, known as the QED cascade [42–44]. It can be triggered for a single pulse with intensity above 10^{25} W/cm^2 [44] or two colliding pulses with intensity above 10^{23} W/cm^2 [45–51]. Therefore, finding out the specific restriction on the attainable laser intensity in these conditions is a key question that needs to be answered for developing lasers beyond 100 PW peak power.

For more realistic consideration, the depletion is a dynamic process where the laser intensity gradually decreases during the development of a QED cascade, which changes the rate of photon emission and pair production. The latter would again deplete the laser energy. A self-consistent dynamic description of the process is therefore required. To this end, we developed a set of dynamic equations that take into account the above-mentioned effects self-consistently. We carried out particle-in-cell (PIC) simulations by including the QED models responsible for the two major reaction channels. Both the simulation and our theoretical model show that the attainable peak intensity depends on the vacuity. At electron density about 10^9 cm^{-3}, notable energy drain emerges from 10^{25} W/cm^2 and the upper limit of the laser intensity is modified to $\sim 10^{26}$ W/cm^2.

2. SIMULATION SETUP

Our investigation is based on two-dimensional (2D) PIC simulations using the code VLPL (Virtual Laser Plasma Lab) [60]. It has implemented a local constant cross-field approximation (LCFA) [35–37,40] QED–Monte Carlo model accounting for nonlinear Compton scattering and Breit–Wheeler processes. Under LCFA, the newly generated particles gain energies from the parent particles rather than directly from the laser photons. The latter transfer their energies when accelerating the leptons. In our simulations, laser propagates from the left side of a moving simulation window along the x direction. The window size is 40 μm (x) × 80 μm (y) resolved by 4000 cells × 1000 cells. We set two macroparticles for electrons and protons in each cell. The laser beam is linearly polarized along the y axis [$E_L = E_G \cos(\omega t - kx)e_y$xz, $B_L = E_G \cos(\omega t - kx)e_z$], following a Gaussian profile $E_G = [aw_0/w(x)]\cos^2[\pi(t - t_f)/2\tau_0]\times \exp[-r^2/w^2(x)]$ focused at $x_f = 240$ μm with normalized peak amplitude $a = eE/m\omega c$ (the corresponding peak intensity $I_{\text{peak}} = (a^2/\lambda^2) \times 1.38 \times 10^{18}$ W/cm^2, with wavelength λ in μm, where m is the mass of electron, c is the velocity of light in vacuum, ω is the laser frequency, and k is the laser wave vector. Here $r^2 = y^2 + z^2$, the laser wavelength is $\lambda = 800$ nm, beam width $w_0 = 3\lambda = 2.4$ μm, $w(x) = w_0\{[(x - x_f)^2 + x_R^2]/x_R^2\}^{1/2}$, Rayleigh length $x_R = \pi w_0^2/\lambda$, focusing time $t_f = x_f/c$, and pulse duration $\tau_0 = 10\lambda/c = 26.7$ fs, respectively. The peak laser field amplitude a is varied from 1500 to 20,000, while the vacuum electron density n_e is tuned between 10^{11} and 10^{15} cm^{-3}. The simulation time step is $\Delta t = 0.008T_0 = 0.008\lambda/c$. In our 2D simulation configuration, the laser pulse is assumed to be uniform in $\delta z = 1\lambda$ finite depth along the z axis. We set periodic boundary conditions for particles such that the latter do not escape from the simulation area after surpassing the z boundary. The particle number counted in a mesh is calculated as $N_r = n_e \times \delta x \delta y \delta z$, where $\delta x = 0.01$ μm and $\delta y = 0.08$ μm are the mesh size.

Two challenges should be addressed while carrying out these simulations: (i) initialization of the low-density electrons and (ii) the memory cost for generated new particles (γ photons and electron–positron pairs). It should be noted that at extremely low electron densities (e.g., 10^{11} cm^{-3}), the average weight of electrons w located in one cell is much less than 1, i.e., it is not physical to start the simulations with simple homogeneous initialization. Therefore, we take the following initialization strategy: first, the particle weight w is calculated once the electron density is given; then, a [0, 1] uniformly distributed random value r_a is generated, by which the weight of the macroparticle is set to $w = \text{int}(w) + \text{rank}(w - r_a)$, where rank is the step function with $\text{rank}(x \geq 0) = 1$, while $\text{rank}(x < 0) = 0$; finally, if $w = 0$, no macroparticles will be placed in the cell. To mitigate the memory issue in simulation, clusters particle merging is turned on when the macroparticle number of one element per cell surpasses 4 [60]. Moreover, modeling the QED cascade processes via the Monte Carlo algorithm and initialization of low-density plasma induce stochastic features. To avoid contingency of the stochastic effects, ten simulation examples with randomly distributed seeds are carried out at each set of parameters.

3. RESULTS AND DISCUSSIONS

We compare the results of $a = 10{,}000$ and 5000 at $n_{e0} = 10^{11}$ cm^{-3} in Fig. 1. The peak laser field amplitude is well preserved for $a = 5000$, as seen in Fig. 1(a). However, it declines to be less than 3000 for the other one. The remarkable difference indicates that the attainable light intensity at $n_{e0} = 10^{11}$ cm^{-3} is subject to strong restrictions, and the upper limit appears at $a = 10{,}000$. The density distributions of electron–positron pairs n_{e+p} and γ photons n_γ are shown in Figs. 1(b) and 1(c), where both are about 3 orders of magnitude higher for the $a = 10{,}000$ case. The density profile shows distinctive patterns between the two cases. We notice that at $a = 10{,}000$, high density bunches appear all along the laser beam, while at $a = 5000$, density peaks are only seen in the vicinity of highest laser intensity. This is because QED cascade is triggered at the rising edge of the laser pulse for the former such that copious electrons and positrons are created at an earlier moment.

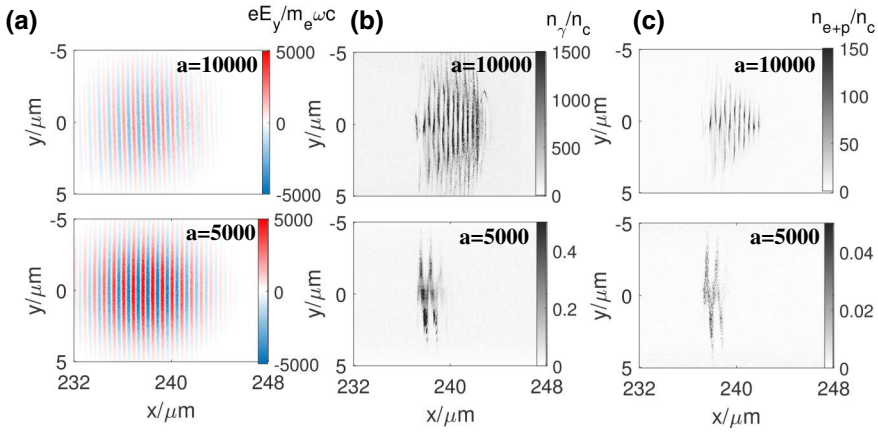

Fig. 1. Distributions of (a) laser electric fields E_y (b) γ photons density n_γ as well as (c) electron–positron density n_{e+p} at $t_f = 300T_0$ and $n_{e0} = 10^{11}$ cm^{-3} for $a = 10000$ (top panel) and $a = 5000$ case (bottom panel), respectively. The E_y is normalized by $m_e\omega c/e$, while densities are normalized by critical density n_c.

When an ultraintense laser interacts with background plasma, the ponderomotive force would usually expel local particles in both longitude and transverse directions. A channel is formed, where the laser pulse propagates through without significant volumetric energy drain. This is not the case in Figs. 1(b) and 1(c). We notice that electrons and positrons, mostly newly generated, sit within the intense laser beam. The corresponding phase-space density of electron–positron pairs is given in Fig. 2 by including the case of $a = 1000$ for comparison. At relatively lower laser intensity ($a = 1000$), transverse momenta dominate over the longitudinal one, meaning that a significant number of electrons are pushed away via laser ponderomotive scattering [see Fig. 2(a)]. The phase-space distribution is drastically different in the case of $a = 5000$ and 10,000. We see that the transverse momenta vanish for majority of the electrons/positrons, manifesting the clustering of leptons along the propagation axis, as displayed in Figs. 2(b) and 2(c). This phenomenon is known as radiation-reaction trapping (RRT) in traveling laser field [33], where the recoiling force of photon emission offsets the pondermotive force, leading to anomalous trapping of leptons in the most intense part of the laser field. It is consistent with the density distribution shown in Fig. 1(b). The threshold of RRT is around $a = 1000$, according to previous studies [33]. In our case, the featured momentum distribution pattern appears when the laser amplitude goes beyond $a = 1000$, in agreement with the theoretical predictions. Note that the RRT threshold is much smaller than the one required to seed a QED cascade. This is particularly important in developing efficient cascading and laser energy depletion. If the thresholds are to be reversed, the generated particles would be expelled from the interaction region and the avalanche-like amplification would not be sustained.

In the following, we derive the theory that describes the evolution of particle numbers from the QED cascade and give the criterion for laser energy depletion. We consider the γ photon and electron–positron pair generation rates satisfying the expression,

$$\frac{\mathrm{d}N_{e+p}}{\mathrm{d}t} = 2\Gamma_e N_\gamma, \tag{1}$$

$$\frac{\mathrm{d}N_\gamma}{\mathrm{d}t} = \Gamma_\gamma N_{e+p} - \Gamma_e N_\gamma, \tag{2}$$

where Γ_e and N_{e+p} are the generated rate coefficient of electron–positron pairs and number of their total particles, correspondingly; Γ_γ and N_γ are the coefficient and number of γ photons, respectively. The generation rate of cascade processes is determined by the QED parameter $\chi_i = |(F_{uv}P_i^v)^2|^{1/2}/E_s m_e c$ $(i = \pm e \text{ or } \gamma)$ [35–37], where F_{uv} is the EM field tensor [61] and P_i^v is the particle's four-momentum. According to previous research, the QED parameter can be approximated by

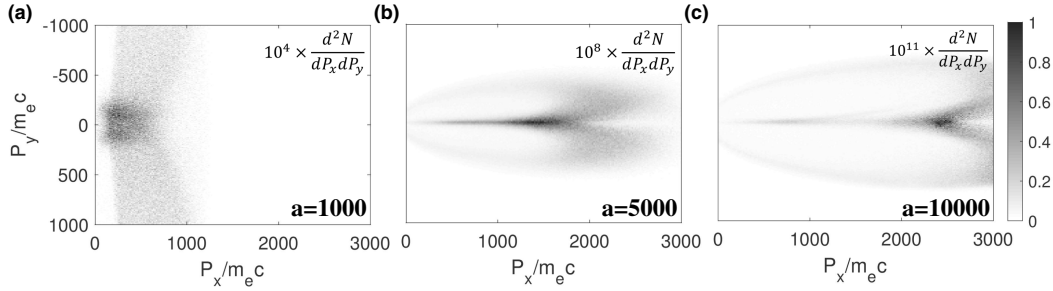

Fig. 2. Electron number density in the momentum space $P_x - P_y$ at focusing time t_f and $n_{e0} = 10^{11}$ cm^{-3} for (a) $a = 1000$, (b) $a = 5000$, and (c) $a = 10{,}000$, respectively. The P_x and P_y are normalized by $m_e c$.

$\chi_i \propto a^{3/2}$ [44], and the generation rate Γ is proportional to $\chi_i^{2/3} \propto a$ [44,45,52]. Considering the generation rate deviating from the $\chi_i^{2/3}$ scaling, especially for small χ values [52], we introduce an exponential modification term $\exp(-a_{\rm ph}/a)$ into the generation rate, i.e., $\Gamma \propto a\ \exp(-a_{\rm ph}/a)$ in our model. The $a_{\rm ph}$ is chosen as $0.01a_s$ (a_s is the normalized Schwinger field), corresponding to the threshold where the cascade occurs. From empirical approximation, the Γ_γ is about $1/T_0$ ($T_0 = \lambda/c$ is the laser period) with $a_{\rm ph} = 0.01a_s$. Combining with the $\Gamma_\gamma \sim 4\Gamma_e$ [52], we obtain the generation rates $\Gamma_\gamma \sim 4\Gamma_e \sim a\ \exp(1\text{-}a_{\rm ph}/a)/(a_{\rm ph}T_0)$. Considering the energy of γ photons and electron–positron pairs is about $am_ec^2/2$ [33,62,63], the laser depletion for such processes can be roughly evaluated as $dE \sim -ad(N_{e+p} + N_\gamma)m_ec^2/2$. Assuming the Gaussian profile remains the same during focusing $a = G(t)\xi = [1 + (t - t_f)^2/t_R^2]^{-1/2}\xi$ and taking $dE \sim 2c_1V_d\xi d\xi/c$ with $t_f = 300T_0$, $t_R = x_R/c = 9\pi T_0$, V_d is the depletion region volume where $a > a_{\rm RRT}$ and $c_1 = m_e^2c^3\omega^2\varepsilon_0/2e^2 = 1.38 \times 10^{18} \times (1\ \mu{\rm m}/\lambda)^2\ {\rm W/cm^2}$, the evolution of ξ is derived as follows:

$$\frac{d\xi}{dt} = -\frac{am_ec^3}{4c_1V_d\xi}(4N_{e+p} + N_\gamma)\Gamma_e. \tag{3}$$

Combining Eqs. (1)–(3) and taking the cascade duration $t_a \sim [(a_0/a_{\rm RRT})^2 - 1]^{1/2}t_R$ (corresponding to the period where $a_0 > a_{\rm RRT}$) with the initial conditions $N_{e+p}(t = t - t_f - t_a/2) = c\tau_0\pi w_0^2 n_{e0}$, $N_\gamma(t = t - t_f - t_a/2) = 0$, the numerical solution of N_{e+p}, N_γ, and a can be acquired. The evolution of N_{e+p} and N_γ based on the above analytical model is given in Figs. 3(a) and 3(b), together with the results collected from PIC simulations. The numbers of both electron–positron pairs and gamma photons undergo exponential growth when the laser interacts with residual electrons, owing to the avalanche-like cascade. When sufficient laser energy is drained, the light intensity declines (see the following discussion in Fig. 4), and the number of created particles saturates. The above trends are reproduced by our theoretical model.

The peak intensity during focusing processes is measured from PIC simulations and compared to our analytical model. Again, the results in Fig. 3(c) illustrate the consistency between the two. According to the systematic scanning, the reduction of peak intensity emerges from 10^{25} W/cm^2, indicating that the depletion effects should be taken into consideration for above a hundred PW class laser facility. The ratio between the simulated peak intensity and the designed intensity decreases sharply when approaching 10^{26} W/cm^2 for density from 10^{11} to 10^{15} cm^{-3}, corresponding to the energy depletion threshold. As seen in Fig. 3(d), when the designed light intensity surpasses the threshold, the attainable one is restricted to 10^{26} W/cm^2 for vacuity down to 10^9 cm^{-3} according to our theoretical model, exhibiting a clear ceiling. The attainable intensity reaches 2×10^{26} W/cm^2 for vacuity $\sim 10^8$ cm^{-3}. It should be noted that at even lower electron densities ($<10^7$ cm^{-3}), the average electron number in the focusing area is less than 1. The cascading effect only occurs when the seeding particle sits in the focal region. In this case, one may not be able to give a definite threshold.

In fact, the rising and falling edges of the laser pulse should be symmetric around $t = t_f$ in the time domain if depletion is negligible. Nevertheless, strong depletion breaks down the

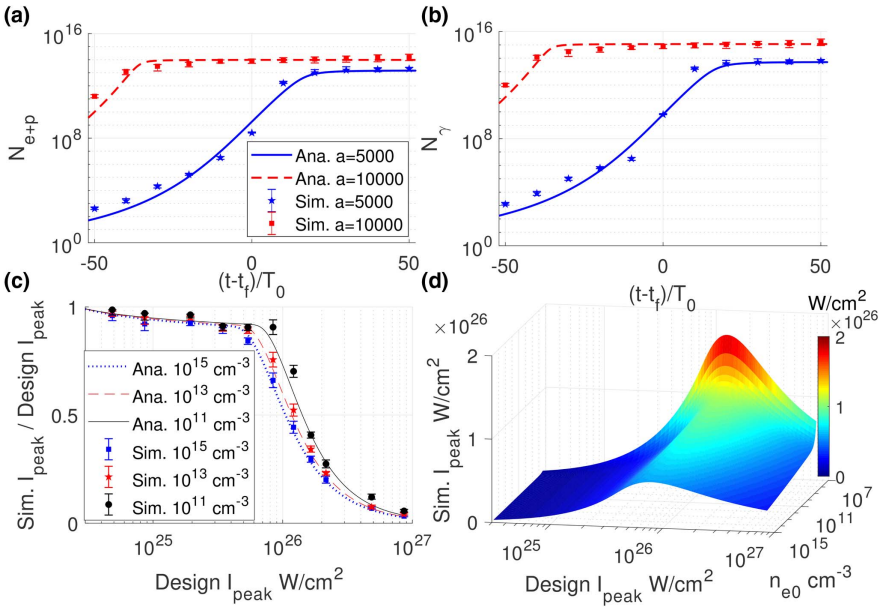

Fig. 3. (a) N_{e+p} and (b) N_γ evolution for $a = 5000$ (blue solid and pentagrams) and $a = 10{,}000$ (red dashed and squares) obtained from simulation (symbols) and theoretical analysis (lines); (c) ratio between the measured peak intensity in simulations and the designed one as a function of designed peak intensity under electron densities of $n_{e0} = 10^{15}$ cm^{-3} (blue dotted and squares), 10^{13} cm^{-3} (red dashed and pentagrams), 10^{11} cm^{-3} (black solid and circles). The symbols are results measured from simulation while lines are from the theoretical model. All symbols represent average values for ten simulation cases with different random seeds, while the error bars represent peak intensity quantile of 95% and 5% (error bar gives a confidence interval of 90%), separately. (d) The theoretical prediction of peak intensity distributions as a function of the designed peak intensity and n_{e0} (from 6×10^7 to 10^{15} cm^{-3}).

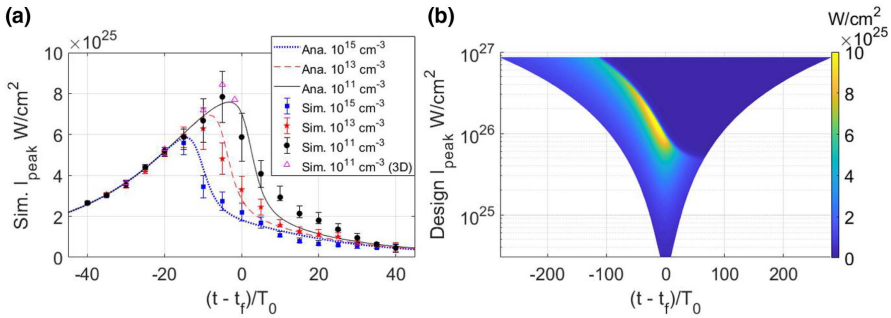

Fig. 4. (a) Obtained peak intensity evolution at $a = 6000$ for different vacuum electron densities n_{e0}. The black circles, red pentagrams, and blue squares represent average peak intensity measured in simulations. The solid black line, dashed red line, and dotted blue line denote theoretical analysis with $n_{e0} = 10^{11}$, 10^{13}, and 10^{15} cm^{-3}, respectively. The pink triangles represent 3D simulation results before simulation memory overflow with $n_{e0} = 10^{11}$ cm^{-3} [a 40 μm (x) × 40 μm (y) × 40 μm (z) window with 2000 cells × 400 cells × 400 cells]. (b) The theoretically predicted peak intensity evolution from analytical model as a function of designed peak intensity at $n_{e0} = 10^{9}$ cm^{-3}.

symmetrical profile such that the maximum intensity observed in simulations is not exactly at the designed focal position. The behavior is even more obvious with higher residual density [Fig. 4(a)] or at intensities beyond the threshold [Fig. 4(b)]. We choose $a = 6000$ as an example and present the peak intensity at different simulation times. As depicted in Fig. 4(a) from both simulations and the theoretical model, the laser peak intensity appears near the focal position for 10^{11} cm^{-3}, while much earlier for the 10^{13} cm^{-3} (by $\sim 10T_0$) and 10^{15} cm^{-3} (by $\sim 15T_0$) cases. Since laser intensity at the pulse rising front does not reach the threshold at 10^{11} cm^{-3}, the distortion caused by depletion is negligible. At higher electron densities, the intensity exceeds the threshold before $t = t_f$ and the cascade develops quickly. Significant depletion in the laser front induces intensity peak shifting to an earlier time than designed. The highest intensity found from simulations as a function of the propagation time is presented from our theoretical model for $n_{e0} = 10^{9}$ cm^{-3}. As one notices in Fig. 4(b), the symmetrical time profile of peak intensity becomes asymmetric when approaching the threshold. In this case, the attainable intensity is restricted to below 10^{26} W/cm^2. Moreover, results of a 3D simulation are also presented in Fig. 4(a) for comparison. Here memory overflow occurs in the later stage due to the enormous number of particles created in the cascade; we therefore show the data before the simulation collapses. One sees the 3D results are in reasonable agreement with the 2D simulations.

It should be mentioned that the cascade process is affected by laser polarization to a certain extent [52]. Since circular polarization essentially requires 3D simulations, we restrain our analysis on linear polarization. One may refer to Ref. [44] for further information on circular polarization. The laser polarization [52], electron seeding [53,54], and saturation [55] can also affect the cascading process. Besides, we employ cos^2 profiles in the time domain as a close approximation to avoid cutoff for Gaussian distribution in simulations. The results between the two profiles show a negligible difference (not shown here). Moreover, the pre-pulse may affect the local electron density at these laser intensities. We take 10^{13} W/cm^2 pre-pulse level with the duration of a nanosecond to estimate the drifting distance due to ponderomotive scattering, which is approximately $\sim a^2 cT/2 \sim 1.5$ μm. The drifting distance is at the same order for picosecond duration laser foot (typically 3 orders of magnitude stronger than the nanosecond pre-pulse). In this case, electrons are still within the laser focal region.

4. CONCLUSION

In summary, we have explored the attainable highest laser intensity under different vacuum conditions for the first time, to the best of our knowledge. It is found that the avalanche-like QED cascade and RRT effect pose a strong limit on the achievable light intensity due to the residual electrons the laser pulses meet. Our study suggests that the observed peak intensity is suppressed starting from $\sim 10^{25}$ W/cm^2, and an upper limit emerges at 10^{26} W/cm^2 for vacuum electron densities above 10^{9} cm^{-3}. These laser intensity thresholds can be approached by focusing the optical laser pulses of multiple hundreds of PW peak power. The cases for building lasers beyond hundreds of PW peak power are therefore not well justified, considering the vacuum conditions for a typical PW-class laser experimental environment.

It is worth noting that light intensities at $\sim 10^{24}$ W/cm^2 can readily support the research on strong-field QED physics (e.g., the radiation-reaction effects, electron–positron pair production, QED cascade), particle acceleration towards the high-energy frontier, laser-driven nuclear physics and high-energy density physics. The featured intensity is already accessible with a 100-PW laser, such as the SEL 100-PW laser under construction in China [64].

Funding. Strategic Priority Research Program of the Chinese Academy of Sciences (XDB 16010000); National Natural Science Foundation of China (11875307, 11935008).

Acknowledgment. The authors would like to thank Prof. Alexander Pukhov for the use of the PIC code VLPL.

Disclosures. The authors declare no conflicts of interest.

REFERENCES

1. D. Strickland and G. Mourou, "Compression of amplified chirped optical pulses," Opt. Commun. **55**, 447–449 (1985).
2. S. W. Bahk, P. Rousseau, T. A. Planchon, V. Chvykov, G. Kalintchenko, A. Maksimchuk, G. A. Mourou, and V. Yanovsky, "Generation and characterization of the highest laser intensities (1022 W/cm^2)," Opt. Lett. **29**, 2837–2839 (2004).
3. V. Yanovsky, V. Chvykov, G. Kalinchenko, P. Rousseau, T. Planchon, T. Matsuoka, A. Maksimchuk, J. Nees, G. Cheriaux, G. Mourou, and K. Krushelnick, "Ultra-high intensity-high contrast 300-TW laser at 0.1 Hz repetition rate," in *Ultrafast Phenomena XVI* (Springer, 2009), pp. 750–752.
4. Extreme Light Infrastructure (ELI), http://www.eli-laser.eu.
5. Z. Guo, L. Yu, J. Wang, C. Wang, Y. Liu, Z. Gan, W. Li, Y. Leng, X. Liang, and R. Li, "Improvement of the focusing ability by double deformable mirrors for 10-PW-level Ti:sapphire chirped pulse amplification laser system," Opt Express **26**, 26776–26786 (2018).
6. N. V. Zamfir, "Extreme light infrastructure–nuclear physics (ELI-NP) European Research Centre," EPJ Web Conf. **66**, 11043 (2014).
7. G. Grittani, C. Lazzarini, S. Lorenz, M. Nevrkla, L. Vilanova, S. V. Bulanov, and G. Korn, "ELI-ELBA: fundamental science investigations with high power lasers at ELI-beamlines," in *High Intensity Lasers and High Field Phenomena* (Optical Society of America, 2020).
8. D. N. Papadopoulos, J. P. Zou, C. Le Blanc, G. Cheriaux, P. Georges, F. Druon, G. Mennerat, P. Ramirez, L. Martin, and A. Freneaux, "The Apollon 10 PW laser: experimental and theoretical investigation of the temporal characteristics," High Power Laser Sci. Eng. **4**, e34 (2016).
9. C. Hernandez-Gomez, S. P. Blake, O. Chekhlov, R. J. Clarke, A. M. Dunne, M. Galimberti, S. Hancock, R. Heathcote, P. Holligan, and A. Lyachev, "The Vulcan 10 PW project," J. Phys. Conf. Ser. **244**, 032006 (2010).
10. R. Li, "Progress of the SULF 10 PW laser project," in *1st AAPPS-DPP Meeting* (2017).
11. D. D. Meyerhofer, S. W. Bahk, J. Bromage, D. H. Froula, D. Haberberger, S. X. Hu, B. E. Kruschwitz, R. L. McCrory, J. F. Myatt, P. M. Nilson, J. B. Oliver, C. Stoeckl, W. Theobald, L. J. Waxer, and J. D. Zuegel, "OMEGA EP OPAL: a path to a 100-PW laser system," in *Meeting of the APS Division of Plasma Physics American Physical Society* (2014).
12. B. Shao, Y. Li, Y. Peng, P. Wang, J. Qian, Y. Leng, and R. Li, "Broad-bandwidth high-temporal-contrast carrier-envelope-phase-stabilized laser seed for 100 PW lasers," Opt. Lett. **45**, 2215–2218 (2020).
13. National Academies of Sciences, Engineering, and Medicine, *Opportunities in Intense Ultrafast Lasers: Reaching for the Brightest Light* (National Academies, 2018).
14. G. A. Mourou, N. J. Fisch, V. M. Malkin, Z. Toroker, E. A. Khazano, A. M. Sergeev, T. Tajima, and B. Le Garrec, "Exawatt-zettawatt pulse generation and applications," Opt. Commun. **285**, 720–724 (2012).
15. G. A. Mourou and T. Tajima, "More intense, shorter pulses," Science **331**, 41–42 (2011).
16. T. Tajima and G. A. Mourou, "Zettawatt-exawatt lasers and their applications in ultrastrong-field physics," Phys. Rev. Spec. Top. Accel. Beams **5**, 031301 (2002).
17. J. P. Palastro, J. L. Shaw, P. Franke, D. Ramsey, T. T. Simpson, and D. H. Froula, "Dephasingless laser wakefield acceleration," Phys. Rev. Lett. **124**, 134802 (2020).
18. J. Schreiber, P. R. Bolton, and K. Parodi, "Invited review article: "hands-on" laser-driven ion acceleration: a primer for laser-driven source development and potential applications," Rev. Sci. Instrum. **87**, 071101 (2016).
19. B. F. Shen, Y. Li, M. Y. Yu, and J. Cary, "Bubble regime for ion acceleration in a laser-driven plasma," Phys. Rev. E **76**, 055402 (2007).
20. L. Yin, B. J. Albright, B. M. Hegelich, K. J. Bowers, K. A. Flippo, T. J. T. Kwan, and J. C. Fernandez, "Monoenergetic and GeV ion acceleration from the laser breakout after burner using ultrathin targets," Phys. Plasmas **14**, 056706 (2007).
21. N. V. Zamfir, "Nuclear physics with 10 PW laser beams at extreme light infrastructure–nuclear physics (ELI-NP)," Eur. Phys. J. Spec. Top. **223**, 1221–1227 (2014).
22. S. Gales, K. A. Tanaka, D. L. Balabanski, F. Negoita, D. Stutman, O. Tesileanu, C. A. Ur, D. Ursescu, I. Andrei, S. Ataman, M. O. Cernaianu, L. D'Alessi, I. Dancus, B. Diaconescu, N. Djourelov, D. Filipescu, P. Ghenuche, D. G. Ghita, C. Matei, K. Seto, M. Zeng, and N. V. Zamfir, "The extreme light infrastructure-nuclear physics (ELI-NP) facility: new horizons in physics with 10 PW ultra-intense lasers and 20 MeV brilliant gamma beams," Rep. Prog. Phys. **81**, 094301 (2018).
23. D. L. Balabanski, R. Popescu, D. Stutman, K. A. Tanaka, O. Tesileanu, C. A. Ur, D. Ursescu, and N. V. Zamfir, "New light in nuclear physics: the extreme light infrastructure," Europhys. Lett. **117**, 28001 (2017).
24. B. A. Remington, D. Arnett, R. P. Drake, and H. Takabe, "Modeling astrophysical phenomena in the laboratory with intense lasers," Science **284**, 1488–1493 (1999).
25. D. R. Farley, K. G. Estabrook, S. G. Glendinning, S. H. Glenzer, B. A. Remington, K. Shigemori, J. M. Stone, R. J. Wallace, G. B. Zimmerman, and J. A. Harte, "Radiative jet experiments of astrophysical interest using intense lasers," Phys. Rev. Lett. **83**, 1982–1985 (1999).
26. B. A. Remington, R. P. Drake, and D. D. Ryutov, "Experimental astrophysics with high power lasers and Z pinches," Rev. Mod. Phys. **78**, 755–807 (2006).
27. F. V. Hartemann and A. K. Kerman, "Classical theory of nonlinear Compton scattering," Phys. Rev. Lett. **76**, 624–627 (1996).
28. A. Di Piazza, K. Z. Hatsagortsyan, and C. H. Keitel, "Strong signatures of radiation reaction below the radiation-dominated regime," Phys. Rev. Lett. **102**, 254802 (2009).
29. G. Lehmann and K. H. Spatschek, "Energy gain of an electron by a laser pulse in the presence of radiation reaction," Phys. Rev. E **84**, 046409 (2011).
30. M. Tamburini, T. V. Liseykina, F. Pegoraro, and A. Macchi, "Radiation-pressure-dominant acceleration: polarization and radiation reaction effects and energy increase in three-dimensional simulations," Phys. Rev. E **85**, 016407 (2012).
31. M. Chen, E. Esarey, C. G. R. Geddes, C. B. Schroeder, G. R. Plateau, S. S. Bulanov, S. Rykovanov, and W. P. Leemans, "Modeling classical and quantum radiation from laser-plasma accelerators," Phys. Rev. Spec. Top. Accel. Beams **16**, 030701 (2013).
32. M. Vranic, J. L. Martins, J. Vieira, R. A. Fonseca, and L. O. Silva, "All-optical radiation reaction at 1021 W/cm^2," Phys. Rev. Lett. **113**, 134801 (2014).
33. L. L. Ji, A. Pukhov, I. Y. Kostyukov, B. F. Shen, and K. Akli, "Radiation-reaction trapping of electrons in extreme laser fields," Phys. Rev. Lett. **112**, 145003 (2014).
34. A. Gonoskov, A. Bashinov, I. Gonoskov, C. Harvey, A. Ilderton, A. Kim, M. Marklund, G. Mourou, and A. Sergeev, "Anomalous radiative trapping in laser fields of extreme intensity," Phys. Rev. Lett. **113**, 014801 (2014).
35. A. I. Nikishov and V. I. Ritus, "Quantum processes in the field of a plane electromagnetic wave and in a constant field. I," Sov. Phys. JETP **19**, 529–541 (1964).
36. V. N. Baier, V. M. Katkov, and V. S. Fadin, *Radiation of Relativistic Electrons* (Atomizdat, 1973).
37. V. Ritus, "Quantum effects of the interaction of elementary particles with an intense electromagnetic field," J. Sov. Laser Res. **6**, 497–617 (1985).
38. A. D. Piazza, C. Müller, K. Z. Hatsagortsyan, and C. H. Keitel, "Extremely high-intensity laser interactions with fundamental quantum systems," Rev. Mod. Phys. **84**, 1177–1228 (2012).
39. G. Breit and J. A. Wheeler, "Collision of two light quanta," Phys. Rev. **46**, 1087–1091 (1934).
40. H. R. Reiss, "Absorption of light by light," J. Math. Phys. **3**, 59–67 (1962).
41. D. L. Burke, R. C. Field, G. Horton-Smith, J. E. Spencer, D. Walz, S. C. Berridge, W. M. Bugg, K. Shmakov, A. W. Weidemann, C. Bula, K. T. McDonald, E. J. Prebys, C. Bamber, S. J. Boege, T. Koffas, T. Kotseroglou, A. C. Melissinos, D. D. Meyerhofer, D. A. Reis, and W. Ragg, "Positron production in multiphoton light-by-light scattering," Phys. Rev. Lett. **79**, 1626–1629 (1997).

42. A. R. Bell and G. K. John, "Possibility of prolific pair production with high-power lasers," Phys. Rev. Lett. **101**, 200403 (2008).
43. G. K. John, A. R. Bell, and I. Arka, "Pair production in counter-propagating laser beams," Plasma Phys. Control. Fusion **51**, 085008 (2009).
44. A. M. Fedotov, N. B. Narozhny, G. Mourou, and G. Korn, "Limitations on the attainable intensity of high power lasers," Phys. Rev. Lett. **105**, 080402 (2010).
45. N. V. Elkina, A. M. Fedotov, I. Y. Kostyukov, M. V. Legkov, N. B. Narozhny, E. N. Nerush, and H. Ruhl, "QED cascades induced by circularly polarized laser fields," Phys. Rev. Spec. Top. Accel. Beams **14**, 054401 (2011).
46. E. N. Nerush, I. Y. Kostyukov, A. M. Fedotov, N. B. Narozhny, N. V. Elkina, and H. Ruhl, "Laser field absorption in self-generated electron-positron pair plasma," Phys. Rev. Lett. **106**, 035001 (2011).
47. C. P. Ridgers, C. S. Brady, R. Duclous, J. G. Kirk, K. Bennett, T. D. Arber, A. P. L. Robinson, and A. R. Bell, "Dense electron-positron plasmas and ultraintense γ rays from laser-irradiated solids," Phys. Rev. Lett. **108**, 165006 (2012).
48. S. S. Bulanov, C. B. Schroeder, E. Esarey, and W. P. Leemans, "Electromagnetic cascade in high-energy electron, positron, and photon interactions with intense laser pulses," Phys. Rev. A **87**, 062110 (2013).
49. S. Tang, M. A. Bake, H. Y. Wang, and B. S. Xie, "QED cascade induced by a high-energy γ photon in a strong laser field," Phys. Rev. A **89**, 022105 (2014).
50. X.-L. Zhu, T.-P. Yu, Z.-M. Sheng, Y. Yin, I. C. E. Turcu, and A. Pukhov, "Dense GeV electron–positron pairs generated by lasers in near-critical-density plasmas," Nat. Commun. **7**, 13686 (2016).
51. M. Jirka, O. Klimo, M. Vranic, S. Weber, and G. Korn, "QED cascade with 10 PW-class lasers," Sci. Rep. **7**, 15302 (2017).
52. V. F. Bashmakov, E. N. Nerush, I. Y. Kostyukov, A. M. Fedotov, and N. B. Narozhny, "Effect of laser polarization on quantum electrodynamical cascading," Phys. Plasmas **21**, 013105 (2014).
53. M. Tamburini, A. D. Piazza, and C. H. Keitel, "Laser-pulse-shape control of seeded QED cascades," Sci. Rep. **7**, 5694 (2017).
54. A. Sampath and M. Tamburini, "Towards realistic simulations of QED cascades: non-ideal laser and electron seeding effects," Phys. Plasmas **25**, 083104 (2018).
55. W. Luo, W.-Y. Liu, T. Yuan, M. Chen, J.-Y. Yu, F.-Y. Li, D. D. Sorbo, C. P. Ridgers, and Z.-M. Sheng, "QED cascade saturation in extreme high fields," Sci. Rep. **8**, 8400 (2018).
56. American Association for the Advancement of Science"So much more to know…," Science **309**, 78–102 (2005).
57. J. Schwinger, *Particles, Sources, and Fields* (Addison-Wesley, 1988).
58. A. M. Fedotov, "Electron-positron pair creation by a strong tightly focused laser field," Laser Phys. **19**, 214–221 (2009).
59. S. S. Bulanov, N. B. Narozhny, V. D. Mur, and V. S. Popov, "Electron-positron pair production by electromagnetic pulses," J. Exp. Theor. Phys. **102**, 9–23 (2006).
60. A. Pukhov, "Particle-in-cell codes for plasma-based particle acceleration," CERN Yellow Reports 1 (2016), p. 181.
61. J. Schwinger, "On gauge invariance and vacuum polarization," Phys. Rev. **82**, 664–679 (1951).
62. I. V. Sokolov, N. M. Naumova, and J. A. Nees, "Numerical modeling of radiation-dominated and QED-strong regimes of laser-plasma interaction," Phys. Plasmas **18**, 093109 (2011).
63. E. Wallin, A. Gonoskov, and M. Marklund, "Effects of high energy photon emissions in laser generated ultra-relativistic plasmas: real-time synchrotron simulations," Phys. Plasmas **22**, 033117 (2015).
64. E. Cartlidge, "Physicists are planning to build lasers so powerful they could rip apart empty space," Science (January 24, 2018), https://www.sciencemag.org/news/2018/01/physicists-are-planning-build-lasers-so-powerful-they-could-rip-apart-empty-space.